
SHIELDING-FREE SIGNAL NOISE SUPPRESSION IN PORTABLE LOW-FIELD MRI

Tran Duc Khang

NUS High School of Math and Science
h2030008@nushigh.edu.sg

Yap Yuan Xi

NUS High School of Math and Science
h1810166@nushigh.edu.sg

ABSTRACT

Portable Magnetic Resonance Imaging (poMRI) setups allow for point-of-care imaging, which can greatly enrich paramedic services. However, these setups are extremely sensitive to external electromagnetic noise. Currently, most poMRIs employ electromagnetic shielding to reduce the external noise, though at the cost of its mobility. This motivates the use of shielding-free techniques. Here we present an approach that uses data recorded from external ambient noise coils to suppress the noise experienced by the primary radio-frequency (RF) receiver coil. Our method boasts a 30-fold noise suppression for individual measurements and a 17-fold average noise suppression for 128 randomly selected samples. Furthermore, our method only requires a calibration time of 56.5 ms, hugely improving on current deep learning methods (which usually require at least 18 minutes to train); thus, allowing for on-the-spot calibration. Our noise suppression method might significantly improve the image quality of poMRI, without the need for a shield.

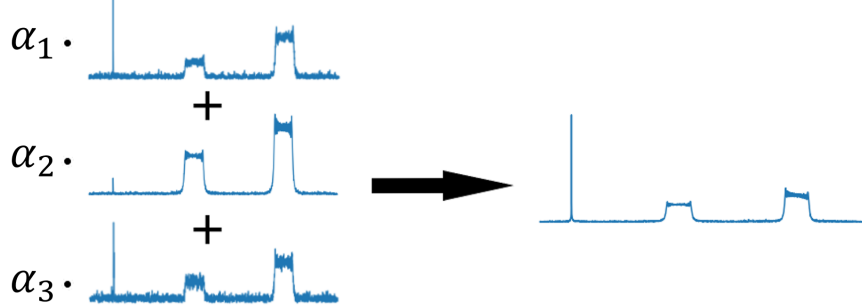


Figure 1: Frequency domain plots of noise experience by noise coils (left) and noise experienced by RF coil (right)

Keywords electromagnetic noise · shielding-free · noise suppression · low-field magnetic resonance imaging

1 Introduction

Magnetic Resonance Imaging (MRI) is one of the best imaging modalities, due to its non-invasiveness and non-ionizing properties. Unfortunately, MRIs are often bulky and costly to maintain, making it inappropriate for point-of-care purposes. As such, there is a lot of active research into portable-MRI (poMRI) setups due to its promises [1].

poMRI often uses smaller permanent magnets (with field strengths ranging from 1-199mT [2]), due to their lower-cost. Because of poMRI very nature, highly sensitive RF detection coils are required; however, this makes the data collected incredibly sensitive to electromagnetic (EM) noise, reducing the signal-to-noise ratio (SNR) of the final image.

However, this trade off can be considered to be desirable as weaker magnetic fields (<25mT) render the noise from the patient's body negligible [3]; whereas for traditional MRIs with stronger magnetic fields (>1T), the body becomes the main source of signal noise that is near impossible to be reduced. Therefore, in using poMRI, we trade an irremediable source of noise for a remediable one. Thus, it is crucial to suppress the external noise, and provide better image quality for poMRIs.

Many LF-poMRI employ Faraday cages surrounding their setup to reduce external EM noise; however, these cages are hindrances to their portability and defeats the purpose of the poMRI. This motivates shielding-free methods of EM noise suppression.

Currently, there are many methods of shielding-free EM noise suppression. Machine Learning Models such as Convolutional Neural Networks (CNN)[4], AutoEncoder[5] and AutoMAP[6] were used to reduce MR Noise. Recently, EM noise suppression via ambient noise coils have been explored [4, 7]. We propose an optimised EM noise suppression method via ambient noise coils, and compared it to existing Machine Learning Models that were used for this specific shielding-free noise suppression idea.

2 Methodology

2.1 Theory

Mathematical Background The signal obtained by the RF coil, s' , can be modelled as a superposition of the desired signal, s , and the undesired electromagnetic interference (EMI), e .

$$s' = s + e$$

Our goal here is to determine, e , from the EMI detected by our noise coils, e'_i for $i \in [1, 2, \dots, N_C]$ with N_C being the number of noise coils.

Now given EMI noise source of frequency, f , moving at non-relativistic speeds, the noise frequency picked up all the coils should all be, f , due to an absence of relativistic Doppler shift. As such, we would expect the frequency domain signal of the noise coils to have the same frequency character as that of the RF receiver coil, though they might have different amplitudes due to different coil positions and orientations. From this we can expect the EMI in the RF coil, e , to be expressible as a linear combination of the EMI detected by the noise coils, e'_i , in frequency domain (Figure 1). From linearity of the Fourier transform, we would expect the same relation to hold in time domain as well

$$\mathcal{F}(e) = \sum_i^{N_C} \mathcal{F}(e'_i) \alpha_i \quad (1)$$

$$\Rightarrow e = \sum_i^{N_C} e'_i \alpha_i \quad (2)$$

We can express (2) as the following matrix equation

$$N \begin{Bmatrix} e_1 \\ e_2 \\ \vdots \\ e_N \end{Bmatrix} = N \left\{ \underbrace{\begin{bmatrix} e'_{11} & e'_{12} & \dots & e'_{1N_C} \\ e'_{21} & e'_{22} & \dots & e'_{2N_C} \\ \vdots & \vdots & \ddots & \vdots \\ e'_{N1} & e'_{N2} & \dots & e'_{NN_C} \end{bmatrix}}_{N_C} \begin{Bmatrix} \alpha_1 \\ \alpha_2 \\ \vdots \\ \alpha_{N_C} \end{Bmatrix} \right\} N_C \quad (3)$$

$$\Leftrightarrow \vec{e} = E' \vec{\alpha} \quad (4)$$

with N being the number of data points sampled, and N_C being the number of noise coils used.

Calibration For a phantom-less acquisition, we would expect our acquired phantomless signal, s_\emptyset' , to be equal to the surrounding EMI, e .

$$s_\emptyset' = e \quad (5)$$

$$\Rightarrow \vec{s}_\emptyset' = E'_\emptyset \vec{\alpha} \quad (6)$$

Thus, as we can find \vec{s}_\emptyset' and E'_\emptyset experimentally, we can determine $\vec{\alpha}$ using the Least-Squares Method to find the $\vec{\alpha}$ that minimizes the objective function over all samples of \vec{s}_\emptyset' and E'_\emptyset , or calibration acquisitions, obtained.

$$\min \|E'_\emptyset \vec{\alpha} - \vec{s}_\emptyset'\|_2 \quad \forall (\vec{s}_\emptyset', E'_\emptyset) \in \Psi_\emptyset$$

with Ψ_\emptyset being the set of all calibration acquisitions.

Noise Suppression After having obtained an optimal $\vec{\alpha}$ for the particular environment, we can use it to determine a synthesized noise signal experienced by the RF coil, e_{syn} , using the EMI data picked up by the surrounding noise coils, E' . Using which, we can suppress the noise, e experienced by the RF coil and recover the desired signal s

$$\vec{e}_{syn} = E' \vec{\alpha} \quad (7)$$

$$\Rightarrow \vec{s} \approx \vec{s}' - \vec{e}_{syn} \quad (8)$$

2.2 Experimental Setup

Noise Coils Construction For noise coils, the more sensitive the better; however, in keeping with the theme of portability, we would want the noise coils to be very small in comparison to the RF receiver coil. After trying different coil designs (Appendix A), we found that a four layer Brooks coil is the most sensitive given our constraints.

We used 1.00mm \emptyset copper wires to construct three 4 layer, 4 turns Brooks coils which has an inductance of 0.16314 μH (Figure 2). This is acceptable as our operating frequency range is high enough to maximise the sensitivity of this device [8]

Data Collection Data is collected from 3 ambient noise coils and one RF receiver coil, all of which are connected to 4 different high frequency channels of RS²D's Cameleon 4 console. The main RF coil is positioned in the rotating Halbach magnet array setup, while the 3 ambient noise coils are held up by adjustable stands flanking the main structure. Their relative positions are shown in Figure 3.

We prepared 3 other coils for synthetic noise generation. The coils are connected to RF generators, 2 of which generate a sweeping frequency between 1.9MHz to 3.5MHz taking 25ms for 1 cycle from 1.9MHz to 3.5MHz and back. The last coil generates a random frequency between 2MHz and 3.5MHz that changes every 10ms. A smaller coil is inserted into the main RF coil to simulate a phantom's signal, we call this the phantom coil. Using these equipment, we collected data with 3 different synthetic noise types both with and without the phantom coil. The synthetic noise types are none, static, dynamic. Static synthetic noise means that our noise generators doesn't move during data collection and dynamic would mean otherwise. This gives us 6 datasets of different types.

We chose to use a phantom coil instead of adding a virtual phantom signal in data processing so that we can better simulate the real situation. For each dataset without the phantom coil we performed 10,000 scans. With the phantom coil, we only performed 1,000 scans. For each scan we collected 2048 points in 1.024 ms, and the phantom coil was kept at 2.84 MHz, which would be the expected magnetic resonance signal emitted by Hydrogen for this setup.

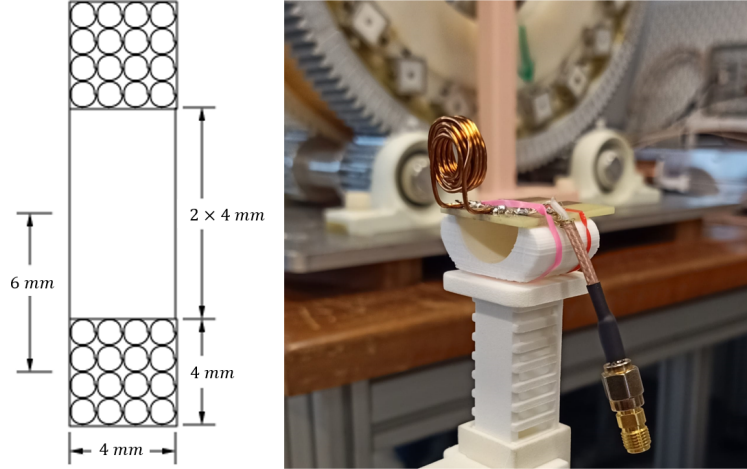
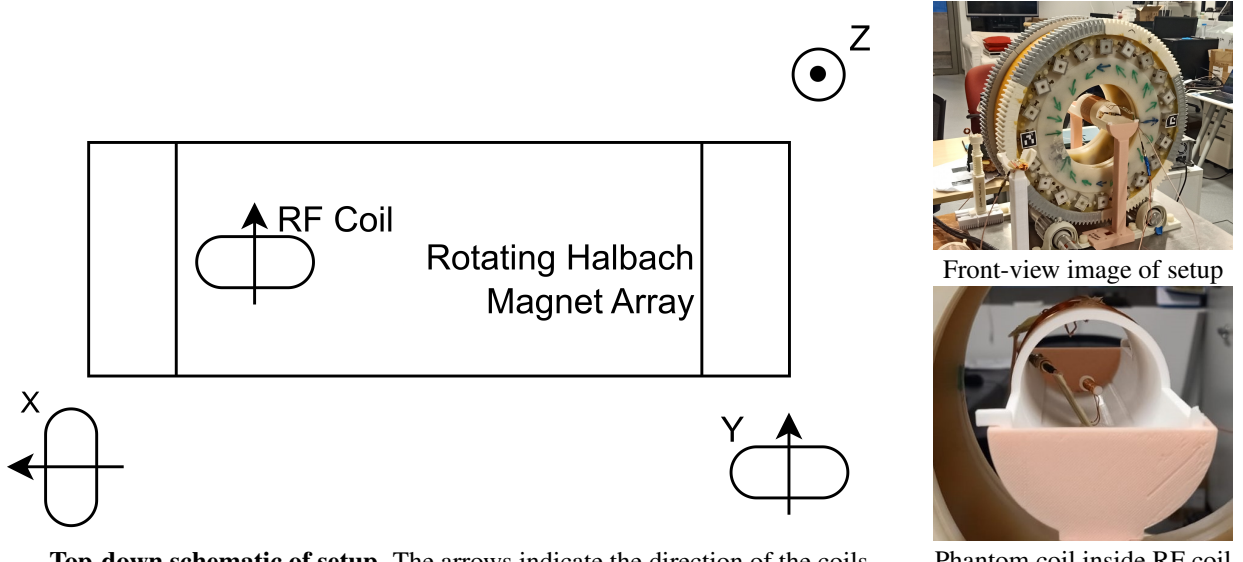


Figure 2: **A schematic of the noise coils and photo of one of them.** Our Brooks coil consists of 4 turns organized into 4 layers, with a wire diameter of 1mm



Top-down schematic of setup. The arrows indicate the direction of the coils

Figure 3: **Experimental setup for data collection**

3 Results

Our method demonstrated a 30-fold noise suppression at the individual measurement level of a randomly chosen sample (Figure 4), and a 17-fold average noise suppression over 128 randomly chosen samples (Figure 5). This is an improvement over the 20-fold, and 16-fold reductions, respectively, demonstrated by Su et. al[4].

In taking these performance measurements, we chose to calibrate $\vec{\alpha}$ on 100 samples immediately before the sample used for evaluation, which took on average $56.5 \pm 4.55\text{ ms}$. This is because we found that the mean absolute loss of our synthesised noise signal settles into a small pocket of stable oscillatory behaviour between 50 and 400 samples, and around 100 samples we encounter our first trough (Figure 5).

We have also demonstrated the model's noise suppression capabilities on a randomly chosen scan with the phantom col. As we can see in Figure 6, all noise signals (i.e. not 2.84 MHz) have been attenuated, with a maximum attenuation of 13-fold.

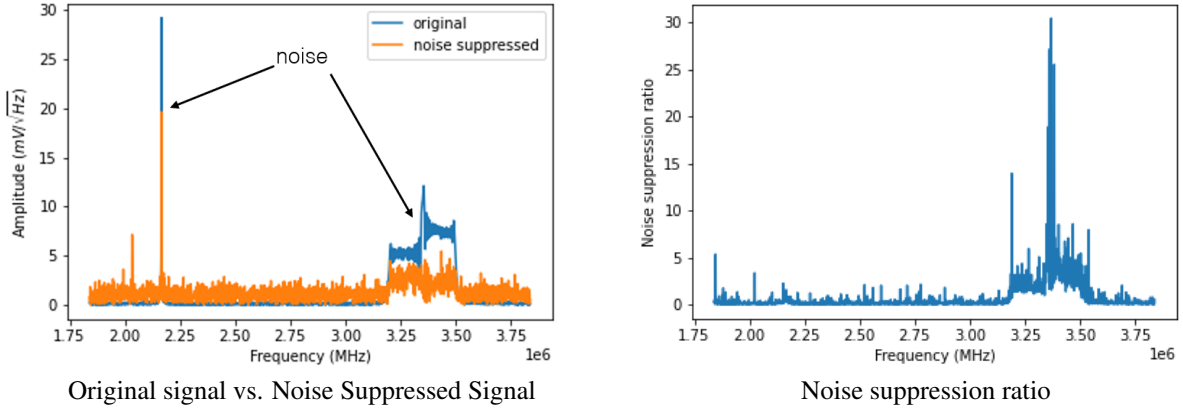


Figure 4: **Matrix noise suppression demonstration for a single phantomless acquisition.** Noise suppression ratio is calculated by dividing the amplitude spectrum of the original signal with its noise-suppressed version

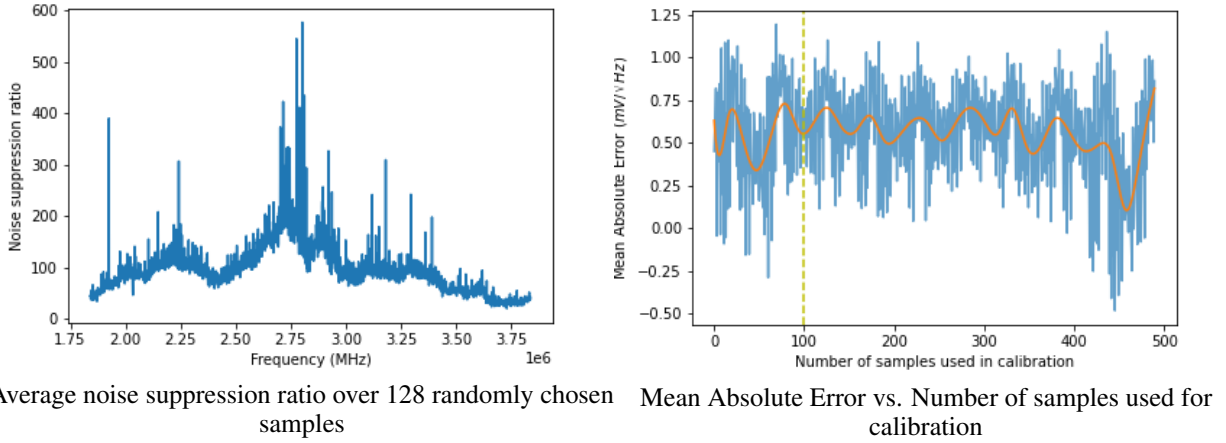


Figure 5

4 Discussion

4.1 Models

To gauge the value of our method, we chose to compare it against two other approaches, the Convolutional Neural Network (CNN) and Linear Regression (LR).

All models were trained using the GPU VM on Google Colaboratory, which had a 16GB Nvidia T4 GPU. Out of the 30,000 phantomless acquisitions, 24,000 was used as training data, and 8,000 was used as hold-out testing data for model comparison.

Convolutional Neural Network We recreated the 7 layer CNN from Su et. al[4] (Figure 7) to pose a fairer comparison to our proposed method as our setup is quite different from their's. To be faithful to [4], we trained the model with Mean Squared Error using Tensorflow Keras

We tested the model on a randomly chosen phantom-less acquisition (Figure 8) and we found that the CNN was able to achieve a 29-fold suppression; however, it also generated virtual noise which is undesirable, as seen in the $3 - 3.5 \text{ MHz}$ frequency band.

Linear Regression This method involves training 2048 linear regression models, each for a certain signal point in time domain. We believed it to be a natural, logical extension of the matrix method presented, as instead of applying the

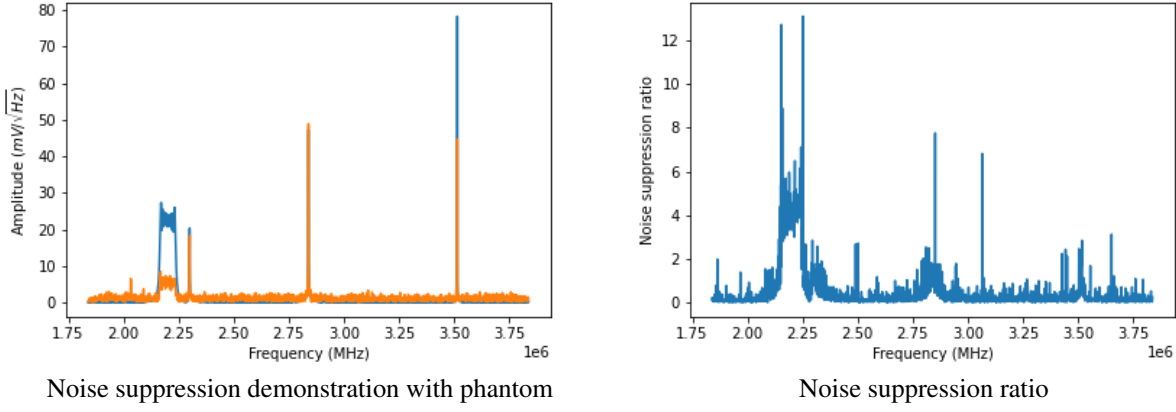


Figure 6: **Matrix noise suppression demonstration for a single phantom-ed acquisition.**

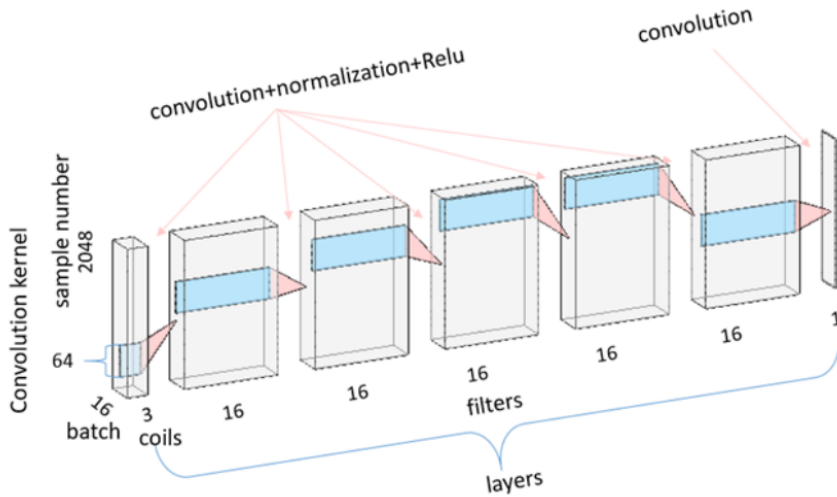


Figure 7: **Diagram of the CNN model used by Su et. al[4], which was taken from their paper**

same N_C coefficients to all 2048 signal points, a separate set of N_C coefficients is used for each signal point. However, it seems that adding parameters negatively affected the performance of the model as it was only able to achieve a 14-fold suppression (Figure 9).

4.2 Comparison

Metric To compare the efficacy of different methods, we chose to use average MAE on frequency domain over 128 randomly selected phantomless samples statistic (or fMAE128 for short). This is because, for our use case, we care more about identifying and correctly suppressing noise frequencies than fitting to the particularities of the signal in time domain. Furthermore, we also included a calibration time statistic, as we wanted to favour models that can be calibrated on the spot. The mentioned statistics for each model is summarised in Table 1.

Table 1: Model Metrics

Model	fMAE128 (mV/\sqrt{Hz})	Calibration time
CNN	1.344	$1081\text{ s} \pm 25\text{ s}$
Linear Regression	1.367	$9.51\text{ s} \pm 447\text{ ms}$
Matrix	1.163	$56.5\text{ ms} \pm 4.55\text{ ms}$

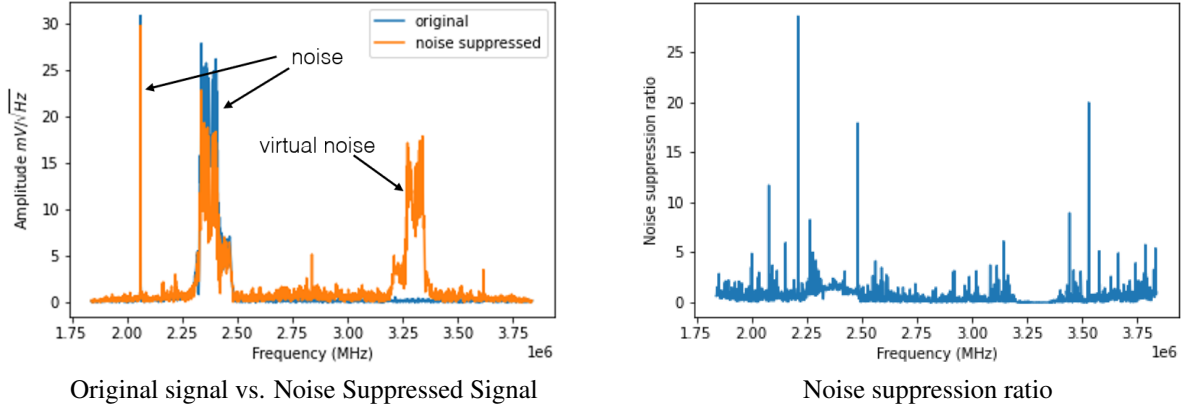


Figure 8: **CNN noise suppression demonstration for a single phantomless acquisition.**

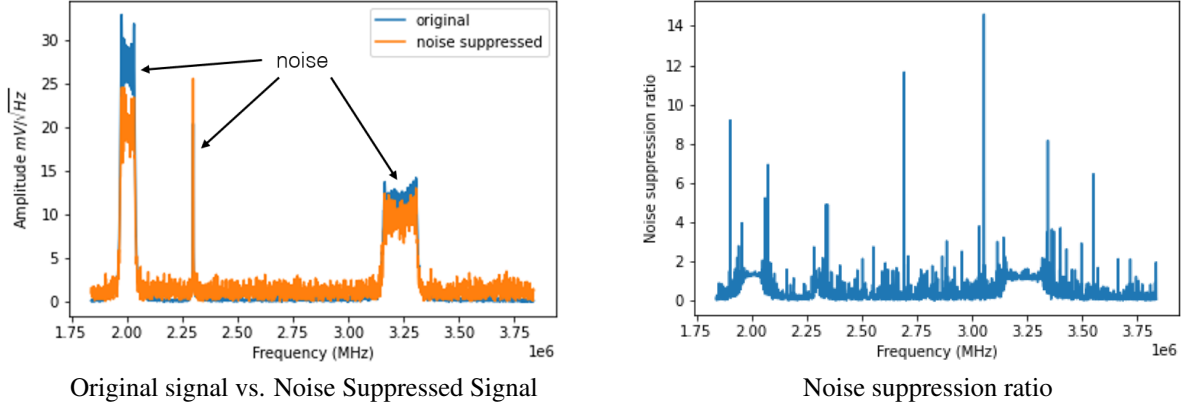


Figure 9: **LR noise suppression demonstration for a single phantomless acquisition.**

Comparison From Table 1, we see that the matrix approach is the best, despite having the least number of parameters. This implies that there exists a form of data consistency between the signal points that is enforced in the matrix approach by applying the same N_C parameters to all of them, and introduction of more parameters caused the models (CNN and LR) to overfit on the training data and thus reduced its performance.

Furthermore, the matrix method requires little calibration time and data, allowing for on-the-spot calibration. This allows it to better fit the peculiarities of the given imaging environment as compared to the CNN approach which takes about 18mins to train and requires at least a few thousand data points to work properly. Therefore, the matrix noise suppression method is a better approach for point-of-care portable MRI services.

5 Conclusion

Signal-to-noise ratio improvements via noise suppression is an important topic in low- and ultra-low-field MRI since these experiments often operate near the limit of detectability and ambient noise can raise the experimental noise floor significantly. Shielding of the electromagnetic environmental noise makes such instruments bulky, and non-portable. To better overcome these limitations, we introduced a shielding-free noise suppression method that can achieve a 30-fold noise suppression for individual measurements and 17-fold average noise suppression over 128 randomly selected samples. Furthermore, we greatly reduced the calibration time, allowing for on-the-spot calibration. Both of which combine to make our method better suited for point-of-care services.

References

- [1] Thomas Arnold, Colbey Freeman, Brian Litt, and Joel Stein. Low-field mri: Clinical promise and challenges. *Journal of Magnetic Resonance Imaging*, 57, 09 2022.
- [2] Mathieu Sarracanie and Najat Salameh. Low-field mri: How low can we go? a fresh view on an old debate. *Frontiers in Physics*, 8, 2020.
- [3] José P. Marques, Frank F.J. Simonis, and Andrew G. Webb. Low-field mri: An mr physics perspective. *Journal of Magnetic Resonance Imaging*, 49(6):1528–1542, 2019.
- [4] Jiasheng Su, Ruben Pellicer-Guridi, Thomas Edwards, Miguel Fuentes, Matthew S. Rosen, Viktor Vegh, and David Reutens. A cnn based software gradiometer for electromagnetic background noise reduction in low field mri applications. *IEEE Transactions on Medical Imaging*, 41(5):1007–1016, May 2022.
- [5] Armando Garcia Hernandez, Pierre Fau, Stanislas Rapacchi, Julien Wojak, Hugues Mailleux, Mohamed Benkreira, and Mouloud Adel. Improving image quality in low-field mri with deep learning. In *2021 IEEE International Conference on Image Processing (ICIP)*, pages 260–263, 2021.
- [6] N. Koonjoo, B. Zhu, G. Cody Bagnall, D. Bhutto, and M. S. Rosen. Boosting the signal-to-noise of low-field mri with deep learning image reconstruction. *Scientific Reports*, 11(1), 4 2021.
- [7] Yilong Liu, Alex T L Leong, Yujiao Zhao, Linfang Xiao, Henry K F Mak, Anderson Chun On Tsang, Gary K K Lau, Gilberto K K Leung, and Ed X Wu. A low-cost and shielding-free ultra-low-field brain mri scanner. *Nature communications*, 12(1):7238, December 2021.
- [8] Kunihisa Tashiro, Shin-Ichiro Inoue, and Hiroyuki Wakiwaka. Sensitivity limits of a magnetometer with an air-core pickup coil. *Sensors & Transducers*, 9:171–181, 12 2010. Copyright - Copyright International Frequency Sensor Association Dec 2010; Document feature - Graphs; Diagrams; Tables; Equations; ; Last updated - 2014-05-22.

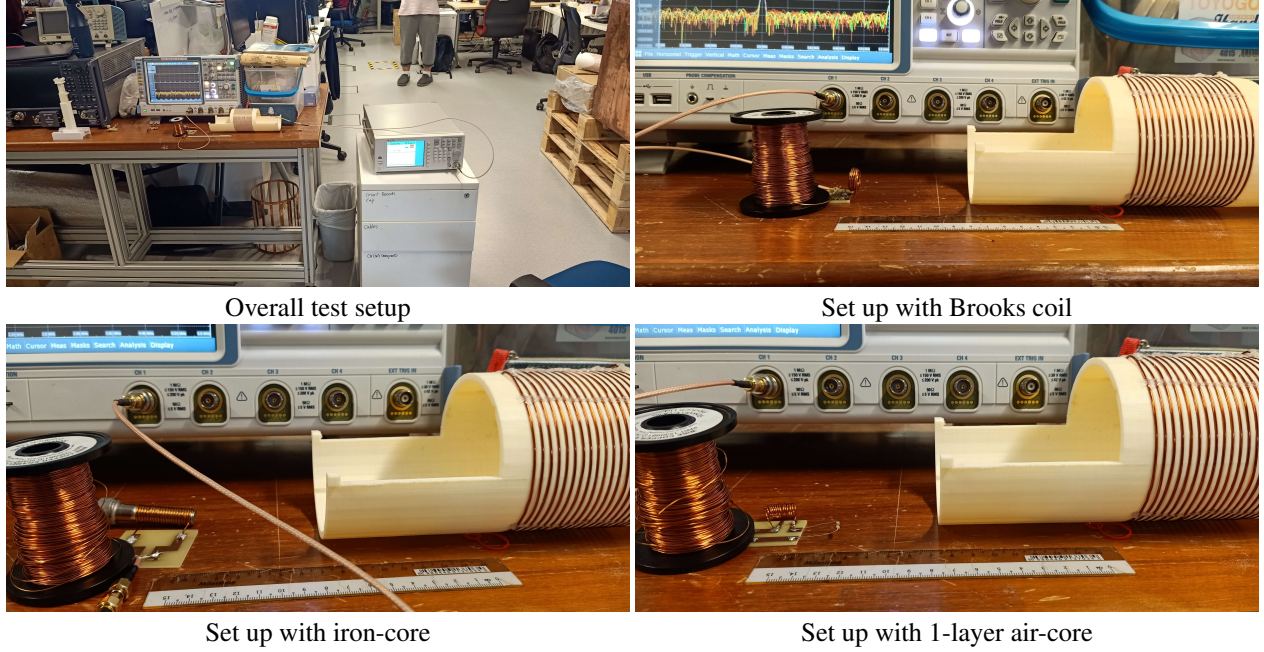


Figure 10: Noise coil sensitivity test setup.

Table 2: Noise coil comparison

Coil Type	Response
Brooks	-44.4 dBm
Iron-core	-70.4 dBm
Air-core (1 layer)	-57 dBm

Appendix

A Noise coil design comparison

To determine the most sensitive noise coil given our constraints, we produced 3 coils (Brooks, iron core, and 1 layer air-core). Our setup consists of a RF coil placed 7.5 cm away from the coil being tested, the two coils are orientated face-to-face. We generated a 2.8 MHz signal using Keysight N9310A RF Signal Generator and recorded the signal picked up by the noise coil using a Rohde & Schwarz Oscilloscope (Figure 10). Our results are summarised in Table 2

B Other Machine Learning Models

Aside from the ones mentioned earlier, we also trained a Long Short-Term Memory (LSTM) model, a two-headed Convolutional LSTM model, a two-headed CNN, and a Feed-Forward Neural Network (FFNN). We found that all the models gave a very low MSE; however, upon sample testing, we find that they either converged to a constant signal profile (for the LSTM, two-headed CNN-LSTM, and two-headed CNN) or failed to synthesize the signal at all (for the FFNN).

Here, "two-headed"-ness refers to the fact that one model excepted both the real and imaginary components as inputs simultaneously (Figure 11), while for the models discussed in the paper, the real and imaginary components are handled by separate models with the same architecture. The fact the two-headed CNN model performed worse than the CNN model suggests that the two streams of data are independently correlated and forcing the model to combine them causes it to become confused and produce the wrong output.

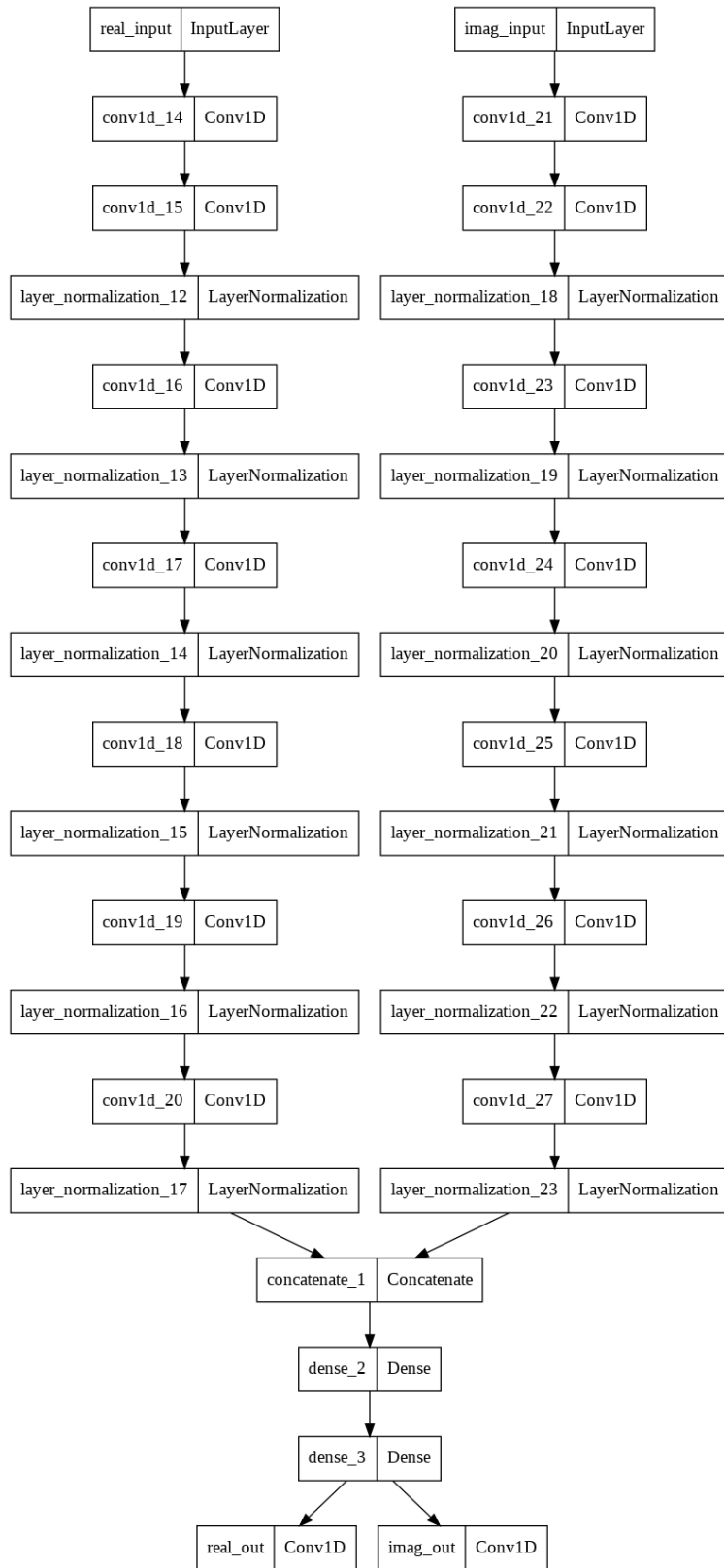


Figure 11: **Diagram of a two-headed CNN**